Hard energy gap and current-path switching in ordered two-dimensional nanodot arrays prepared by focused electron-beam-induced deposition

Roland Sachser,* Fabrizio Porrati, and Michael Huth
Physikalisches Institut, Goethe-Universität, Max-von-Laue-Str. 1, 60438 Frankfurt am Main, Germany
(Received 4 August 2009; revised manuscript received 30 September 2009; published 18 November 2009)

We present electronic transport measurements on ordered two-dimensional nanodot arrays with dot diameters of about 20 nm prepared by focused electron-beam-induced deposition (FEBID). Low-temperature conductance measurements and I/V characteristics strongly indicate that single electron transport through the nanodot arrays is dominated by the charging energy of the individual nanodots. From the I/V characteristics we infer the existence of a hard energy gap or threshold voltage V_t. This is supported by the observed Arrhenius behavior of the low-temperature conductance in the temperature range from 1.8 K to about 60 K. The hard energy gap indicates that electrostatic disorder in our samples is weak and that the granular arrays are in the ordered limit. In contradistinction to other preparation techniques, FEBID makes a continuous tuning of the intergranular coupling strength possible, even through a metal-insulator transition. From time-dependent current measurements at fixed bias voltage we infer that current flow through the nanodot arrays near threshold is through a narrow channel. At larger bias voltage channel branching occurs. The resulting dependence of $I(V)$ is in excellent agreement with theoretical studies on collective charge transport in arrays of small metallic dots.

DOI: 10.1103/PhysRevB.80.195416 PACS number(s): 73.23.Hk, 71.30.+h, 73.22.−f, 81.07.−b

I. INTRODUCTION

Nanodot arrays are versatile model systems for studying charge transport phenomena on the mesoscopic scale. At sufficiently low temperatures, $k_BT \leq E_C/3.5$, the charging energy E_C of an individual dot induces correlation effects in electronic transport.

On the preparational side, for metallic nanodot systems a well-proven technique is codeposition of metal and insulator under conditions which favor phase segregation.[1] This necessarily implies a large degree of disorder in the resulting granular metals which leads to serious difficulties in the theoretical analysis since a fully appropriate theoretical approach would have to take correlation effects and disorder into account on an equal basis.[2] Close to a disorder- or correlation-driven metal-insulator transition (MIT) this difficulty is most pronounced. For ordered systems, on the other hand, the theoretical analysis is facilitated albeit it is still a demanding task to properly take correlation effects into account.[2]

Periodic granular arrays represent such ordered systems. The grains in these arrays in the insulating regime are weakly coupled to their neighbors. Transport takes place by tunneling between two grains. If an electron tunnels from one grain to another, it has to overcome a Coulomb energy, corresponding to the charging energy E_C of a grain. At low temperatures, this Coulomb energy blocks the transport and leads to a hard energy gap at the Fermi level.

Due to the hard energy gap the arrays should show Arrhenius behavior in the temperature dependence of electrical conductance. This is mostly not observed. In many experiments a stretched-exponential dependence of conductance on temperature, the so-called Efros-Shklowski variable-range hopping with exponent 1/2, is found instead.[3] Random variations in the capacitance due to grain-size dispersion was given as a first explanation of this behavior.[4] But later experiments showed the stretched-exponential temperature dependence also on samples in which the size dispersion and distance deviation was highly controlled.[3]

The current theory discusses two reasons, which are thought to be responsible for the Efros-Shklowski-type variable-range hopping: electrostatic disorder and cotunneling. Electrostatic disorder by carrier traps in the matrix or substrate lifts the Coulomb blockade of adjacent grains and increases the density of states at the Fermi level. Cotunneling enables tunneling between two grains over distances larger than the average distance of two granules via virtual states in grains in between. These two reasons lead to a pseudogap in the density of states with $D(\epsilon) \sim \epsilon^2$ at the Fermi level resulting in a stretched-exponential dependence of conductance on temperature instead of Arrhenius behavior for a hard energy gap.

As a consequence, preparation techniques which can yield ordered nanodot arrays and which have control over the type and degree of disorder in the array are attractive. In this regard the technique of crystallization of nanocrystals, mainly Au, from colloidal suspensions has been shown to provide a qualified approach.[5–7] The molecular structure and steric demand of the organic ligands at the nanoparticles' surfaces determine the interdot coupling strength. Such prepared dot arrays are quite generally found to be on the insulating side of the MIT, i.e., the electrical conductance shows activated behavior and tends to zero for $T=0$.[8] A continuous tuning of the coupling strength in these systems, especially into the metallic regime, is difficult. Furthermore, electrostatic disorder in the insulating matrix has a strong influence on the electronic transport properties and can eventually destroy the hard energy gap at the Fermi level.

A different approach is taken by the technique of focused electron-beam-induced deposition (FEBID). In FEBID a highly focused electron beam, most commonly provided by a high-resolution scanning electron microscope (SEM), is rastered over a substrate surface which is covered by a physisorbed and volatile molecular metal-organic layer. As the

electron beam fractures the molecules a permanent deposit is formed. Volatile dissociation products desorb and are removed from the SEM by the pumping system. For a recent review on this technique see Ref. 9. For most metal-organic precursors and under a wide range of beam parameters the resulting deposits are disordered granular metals containing metallic nanocrystals, with typical size in the few nm range, embedded in an insulating and carbon-rich matrix. FEBID has advantages as compared to the codeposition technique insofar, as it allows for a precise control of the deposits' lateral dimensions in the 10 nm range or even below.[10] The disordered state of the deposits, however, poses the same problems as have been encountered in granular metals prepared by the codeposition technique, although interesting transport behavior on the metallic side of the MIT has been observed in FEBID structures.[11]

Here we utilize FEBID for the preparation of ordered two-dimensional square arrays of metallic dots with a diameter of about 20 nm and center-to-center distance a (pitch). This process allows a continuous tuning of the intergranular coupling strength. By varying a between 25 and 40 nm we obtain dot arrays on either side of the MIT. We then focus on analyzing the electrical conductance in these arrays as a function of temperature and we analyze the I/V characteristics and time-dependent current measurements in the theoretical framework of electrostatic energy minimization, as was developed by Middleton and Wingreen[12] and further refined by Jha and Middleton.[13] The samples in the insulating regime show Arrhenius behavior, which indicates the existence of a hard energy gap. This hard energy gap at the Fermi level is evidence that electrostatic disorder in our samples is weak and that we do not have cotunneling in our samples.

II. EXPERIMENT

As a substrate for the FEBID dot arrays p-doped silicon with a 300 nm thermally grown SiO_2 layer was used. 120 nm Cr/Au contacts were prepared by UV lithography and lengthened by ion-beam-induced deposition to define a gap of about 1 μm between the electrodes. Over this gap the dot arrays were prepared using FEBID. We employed a Nova Nanolab 600 SEM with a Schottky-type emitter. The SEM is equipped with several gas injection systems. We used $W(CO)_6$ as precursor gas, which was transported to the focal area of the electron beam through a small capillary with 0.5 mm diameter. A beam current of 1.6 nA and an acceleration voltage of 5 kV were chosen to secure a high metal content, $x \gtrsim 40\%$, in the deposits. The immersion mode of the SEM was used during deposition to achieve high resolution at the relatively small energy of 5 keV. The full width at half maximum of the Gaussian beam profile amounts to ~ 20 nm under these conditions. This also defines the diameter of the resulting FEBID dots at each individual dwell point.[9] To get arrays a rastering process was used. Samples with a of 25, 30, and 40 nm at a dwell time of 1 ms were prepared. Each dot array pattern was iterated 20 times resulting in a dot height of about 15 nm as deduced from selected atomic force microscopy scans. Linescans of SEM images were performed to measure the dot diameter. An error margin of 2 nm is caused by the discrete pixels of the SEM image and not by the deposition process. So the size dispersion of the dots is less than 10% (2 nm). The center-to-center deviation is limited by the resolution of the pattern generator of the used SEM, in our case less than 1 nm. Table I gives an overview over the geometric key parameters of the dot arrays. A sample with 40 nm center-to-center distance is shown in the inset of Fig. 2. Due to the Gaussian beam profile each dot can be assumed to have a similar Gaussian profile. At the same time, the metal content in each dot is largest at the maximum of the beam profile. From the tails of the Gaussian beam an insulating deposit results, with a very small or no metal content. Via this part of the deposit the central metal-rich region of each dot is electrically coupled to its next neighbors. For electrical transport measurements the samples were mounted in a variable temperature insert in a ^{4}He cryostat. The time between venting the SEM and mounting the samples to the cryostat was kept as short as possible to minimize aging effects.[14] A Keithley Sourcemeter 2400 was used to apply a fixed bias voltage resulting in an electrical field of 50–100 V/cm for the temperature-dependent conductance measurements. The time-dependent current measurements at fixed bias were done with a resolution of about 15 measurements per second over a time scale of about 15 min.

TABLE I. Overview over geometric key parameters of the prepared dot arrays. The dot diameter is measured by a linescan of a SEM picture. An error of 2 nm in the dot diameter results from the discrete pixels.

Sample	1	2	3
a	25 nm	30 nm	40 nm
Dot diameter	17 nm	20 nm	22 nm
Width	21 dots	17 dots	13 dots
Length	37 dots	34 dots	24 dots

III. RESULTS

In Fig. 1 the temperature-dependent conductance S of samples 1–3 is shown. Concluding metallic or insulating behavior by simple extrapolation of $S(T)$ to $T=0$ can be misleading. The logarithmic derivative $w = d \ln S / d \ln T$ gives a more accurate criterion.[15] Insulating behavior is indicated by $w > 0$ for $T=0$ in contrast to metallic behavior, which leads to a vanishing w as $T=0$ is approached. The logarithmic derivatives w are plotted in the inset. Sample 3 is clearly showing insulating behavior, sample 1 is metallic, and sample 2 appears to be near the MIT.

Sample 3 follows an Arrhenius law $S \sim \exp(-T_0/T)$ in the range 16–60 K as plotted in Fig. 2. The activation temperature $T_0 = 143.3$ K of sample 3 corresponds to an energy of 12.4 meV. For sample 2 no Arrhenius law is observed.

In Fig. 3 the current-voltage characteristics for samples 2 and 3 at several temperatures are shown. Sample 3 shows a threshold voltage V_t at low temperatures. The current follows a power-law dependence of the form $I \sim (V - V_t)^{\zeta}$. We determine the threshold voltage and exponent by dividing the current by dI/dV so that

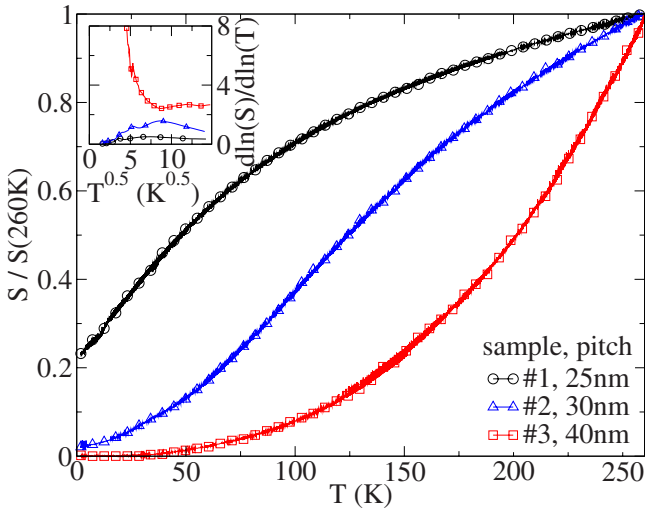

FIG. 1. (Color online) Temperature-dependent conductance S for samples with center-to-center distance as indicated. Inset: logarithmic derivative $w=d\ln S/d\ln T$ showing insulating behavior for sample 3 and metallic behavior for samples 1 and 2.

$$\frac{I}{dI/dV} = \frac{1}{\zeta}(V - V_t) \tag{1}$$

and making a linear regression. The threshold voltages and the exponents for different temperatures are plotted in the insets of Fig. 3(a). The threshold voltage decreases linearly with increasing temperature. Extrapolation of the threshold voltage gives for zero temperature $V_t(T\rightarrow 0)=98.2$ mV. The exponent of the power-law dependence raises slightly from 1.66 to 1.78 with temperature.

Figure 4 depicts a selection of time-dependent current measurements at fixed bias for samples 2 and 3 at 4.2 K. On the left side $I(t)$ is depicted. From previous experiments we know that FEBID structures are susceptible to aging if exposed to air under ambient conditions.[14] This leads to a reduction in the coupling strength between the metallic grains. We used this to enhance the threshold voltage of sample 3. After 3 h of exposure to air V_t was found to be 224 mV at 4.2 K. Below V_t at 200 mV no current flow is detectable. Above V_t we see different discrete current levels, which are sometimes stable for more than 20 s (300 data points). At higher bias voltages the frequency of these switching processes increases and the steps get smaller relative to the average current. The histograms on the right of Fig. 4 show the abundance of measured current values around the average current. For sample 3 the histograms show for bias voltages of 300 and 400 mV two discrete current states. At higher bias voltages this is no longer observed. Interestingly, also sample 2, which is near the MIT, shows this switching between different current distributions. It exhibits three discrete states for 20 and 30 mV bias as is evident from the histograms. At higher bias these peaks vanish.

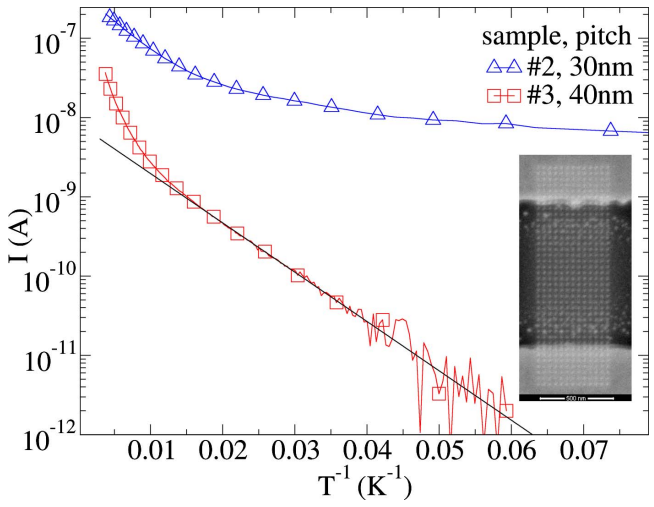

FIG. 2. (Color online) Temperature-dependent conductance for samples 2 and 3. Sample 3 with $a=40$ nm shows Arrhenius behavior. Inset: SEM image of sample 3.

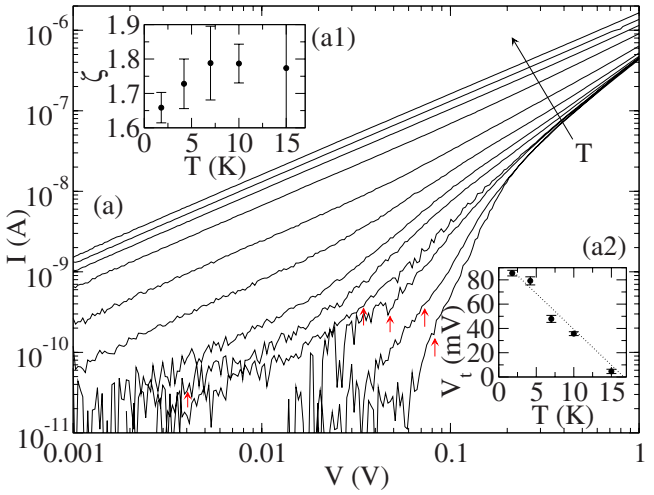

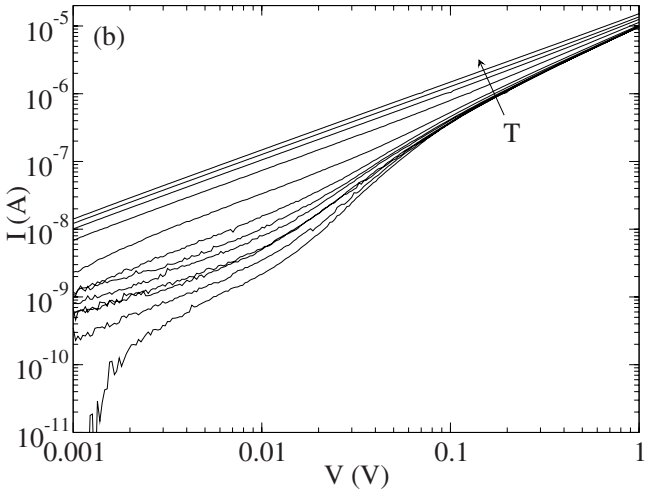

FIG. 3. (Color online) (a) $I(V)$ curves for sample 3. For low temperatures the curves show a threshold voltage (small red arrows) and the current follows a power-law dependence $I\sim(V-V_t)^{\zeta}$, (a1) exponent ζ of power law, (a2) temperature-dependent threshold voltage V_t, and (b) $I(V)$ curves for sample 2.

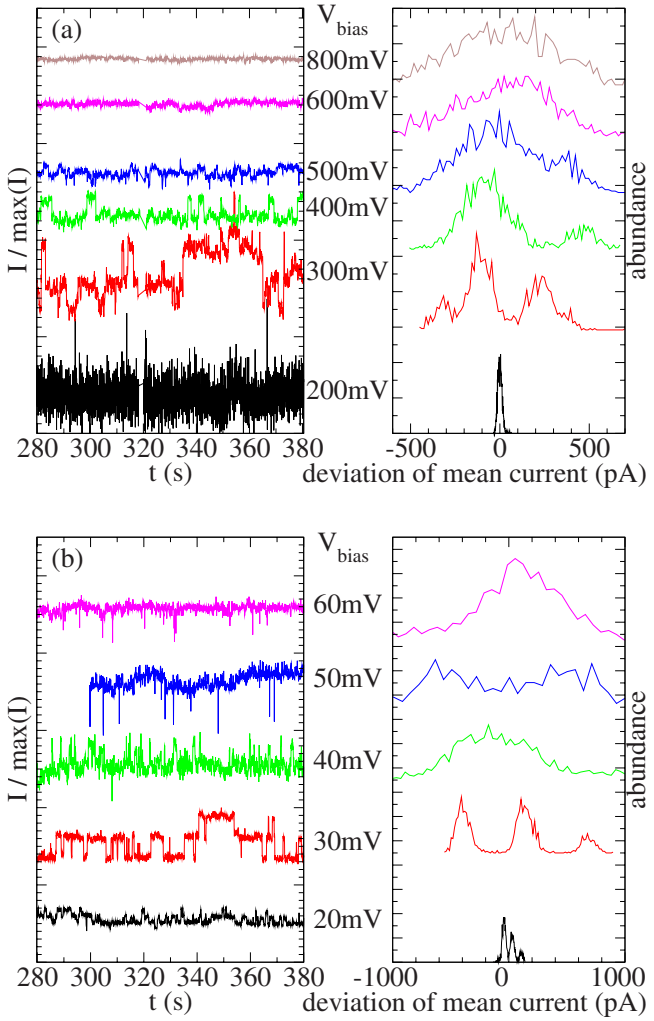

FIG. 4. (Color online) (a) Sample 3, (b) sample 2, left side: a part of the performed time-dependent current measurements at different fixed bias voltages at 4.2 K. For voltages higher than the threshold voltage switching between different discrete current levels occurs. This is related to the fact that at these voltages the transport is not taking place over the whole width of the sample but through one or a few current paths. Right side: histograms of time-dependent measurements which show for certain bias voltages different active current paths through the sample. Different bias voltages are shifted vertically for better visibility.

IV. DISCUSSION

Energy-level quantization in the dots is negligible in our experiments. The mean energy-level spacing is $\delta=\frac{1}{N_F V}$ with density of states at the chemical potential N_F and dot volume V. For our samples we estimate $\delta\approx 3.5\ \mu\text{eV}\approx 40$ mK, so we are still in the "classical" regime. The Arrhenius behavior of the temperature dependence of the conductance of sample 3 is indicative for a hard energy gap at the Fermi level caused by Coulomb interactions in a highly ordered system. Theory predicts for this temperature dependence $S=2S_0\exp(-E_C/k_BT)$.[2,16] If we assume a Gaussian shape for the metal-rich part of each dot the capacitance for a sphere with the same volume (diameter 25 nm) and an assumed static dielectric constant $\epsilon=4$,[14] the capacitance of a dot is 5.6 aF. This corresponds to a charging energy of $E_C=e^2/2C=14.3$ meV. This is in good agreement with the measured activation energy $k_BT_0=12.4$ meV.

It must be stressed here that FEBID structures prepared with strongly overlapping dwell areas form disordered, granular metals. In particular, they show, in contrast to the arrays, an Efros-Shklowski-type variable-range hopping with $S\sim\exp[-(T_0/T)^{1/2}]$ which—as detailed before—is thought to be caused by electrostatic matrix disorder and higher-order contributions to the tunneling process involved.[11] From this we conclude that the observed hard energy gap, which is in good correspondence with the estimated charging energy, is due to the geometric parameters of the nanodot array itself and not due to a possible subgranular structure of each individual dot.

We now focus on samples 2 and 3 and discuss the electrical transport by analyzing the I/V characteristics and $I(t)$ measurements at fixed bias voltage. The temperature-dependent conductance of sample 1, which is clearly showing metallic behavior, will be discussed in a separate publication.

Middleton and Wingreen describe the transport through an array of metallic dots, which are capacitively coupled to their next neighbors and to the back gate.[12] Only first-order contributions to the tunneling process are considered. Theory predicts a power-law dependence of the I/V characteristics of the form $I\sim(V-V_t)^{\zeta}$. V_t is a threshold voltage at zero temperature $V_t(0)=\alpha NV_0$ with $\alpha=0.338$ for square arrays, N the number of dots along the array and eV_0 the charging energy. The conductance at $T=0$ is zero for voltages below V_t. For two-dimensional arrays an exponent of 5/3 is predicted by theory and numerical simulations.[12,13]

We find for sample 3 a power-law dependence as described by Middleton and Wingreen.[12] This supports the conclusion about the existence of a hard energy gap at the Fermi level. With $V_t(T\rightarrow 0)=98.2$ mV and $N=24$ follows for sample 3 $eV_0=12.1$ meV. This is in excellent agreement with the value calculated by the activation temperature of the Arrhenius law (12.4 meV) and the value calculated by the capacitance calculations (14.3 meV). The linear decrease in V_t is similar to the findings of Parthasarathy *et al.*[6] in experiments on Au nanocrystal arrays grown from colloidal solutions. The exponent of the power law found in our experiments is in the range 1.66–1.78, which is similar to the predicted value 5/3.

Higher-order tunneling contributions, i.e., multiple cotunneling, as seen in experiments on Au nanocrystal arrays grown from colloidal solution, are not relevant in our case. Cotunneling would prevent a threshold voltage. In the cotunneling regime the exponent of the power-law dependence of the I/V characteristics should be equal to 1 for low voltages and at higher voltages larger than 3.[3] The results show that the classical description of Middleton and Wingreen, which takes only first-order tunneling contributions into account, is applicable to the measurements of the presented arrays. In this case, switching between different current paths or branching of the active current path should be observable. Theory predicts that at voltages slightly above V_t only one current path associated with minimal electrostatic energy is active. Increasing the voltage, branching of this path or

switching to another path with smaller electrostatic energy will occur. Increasing the voltage further, several active current paths are formed until, at even larger bias, the current flows over the complete sample cross section.

Our measurements show this switching behavior between different current paths. The histograms in Fig. 4 show for sample 3 two discrete states for 300 and 400 mV bias. For sample 2 three discrete states for 20 and 30 mV bias are distinguishable. This is due to switching between different active paths or branching of one currently active path. The height of the steps relative to the average current (25% for sample 3 at 300 mV) indicates that only one or a few current paths are active. At higher bias switching is no longer observable and denotes that at this bias the current flows through many active current paths or the whole sample cross section. This current-path switching is comparable to the experimental findings of Elteto *et al.*[5] on colloidal Au crystals and shows again the good agreement with the model of Middleton and Wingreen.[12]

V. CONCLUSIONS

In conclusion, we have shown that focused electron-beam-induced deposition allows for the preparation of two-dimensional granular arrays in the ordered limit. In electronic transport results obtained on systems prepared with other techniques, such as crystal growth from colloidal solutions, are reproduced. An important aspect is that our method allows for continuously tuning through the MIT by varying the arrays lattice constant as this adjusts the interdot coupling strength. Controlling the raster process, this technique also facilitates studies on the influence of disorder. Smaller diameters and interdot spacing, down to the sub-10 nm range, can be achieved by using higher acceleration voltages and/or smaller beam currents.[10] The results presented here show that for samples with dot diameters of about 20 nm the classical limit of electronic transport in ordered arrays, which is covered by the theory of Middleton and Wingreen, is addressable. Even samples at the MIT show switching behavior which is explained by this theory. This type of switching effects are not taken into account in field-theoretical approaches to the transport problem in granular arrays.[2,16] These approaches, on the other hand, factor in higher-order tunneling contributions. Experimentally it will be both, challenging and rewarding, to extend the studies presented here to nanodot arrays with smaller dot diameters and interdot spacing. Work along these lines is in progress.

ACKNOWLEDGMENTS

Financial support by the NanoNetzwerkHessen (NNH) and by the Bundesministerium für Bildung und Forschung (BMBF) under Grant No. 0312031C is gratefully acknowledged.

*sachser@physik.uni-frankfurt.de

[1] P. A. Lee and T. V. Ramakrishnan, Rev. Mod. Phys. **57**, 287 (1985).
[2] I. S. Beloborodov, A. V. Lopatin, V. M. Vinokur, and K. B. Efetov, Rev. Mod. Phys. **79**, 469 (2007).
[3] T. B. Tran, I. S. Beloborodov, X. M. Lin, T. P. Bigioni, V. M. Vinokur, and H. M. Jaeger, Phys. Rev. Lett. **95**, 076806 (2005).
[4] B. Abeles, P. Sheng, M. Coutts, and Y. Arie, Adv. Phys. **24**, 407 (1975).
[5] K. Elteto, X. M. Lin, and H. M. Jaeger, Phys. Rev. B **71**, 205412 (2005).
[6] R. Parthasarathy, X. M. Lin, K. Elteto, T. F. Rosenbaum, and H. M. Jaeger, Phys. Rev. Lett. **92**, 076801 (2004).
[7] R. Parthasarathy, X. M. Lin, and H. M. Jaeger, Phys. Rev. Lett. **87**, 186807 (2001).
[8] R. P. Andres, J. D. Bielefeld, J. I. Henderson, D. B. Janes, V. R. Kolagunta, C. P. Kubiak, W. J. Mahoney, and R. G. Osifchin, Science **273**, 1690 (1996).
[9] I. Utke, P. Hoffmann, and J. Melngailis, J. Vac. Sci. Technol. B **26**, 1197 (2008).
[10] L. van Kouwen, A. Botman, and C. W. Hagen, Nano Lett. **9**, 2149 (2009).
[11] M. Huth, D. Klingenberger, C. Grimm, F. Porrati, and R. Sachser, New J. Phys. **11**, 033032 (2009).
[12] A. A. Middleton and N. S. Wingreen, Phys. Rev. Lett. **71**, 3198 (1993).
[13] S. Jha and A. A. Middleton, arXiv:cond-mat/0511094 (unpublished).
[14] F. Porrati, R. Sachser, and M. Huth, Nanotechnology **20**, 195301 (2009).
[15] A. Möbius, Phys. Rev. B **40**, 4194 (1989).
[16] K. B. Efetov and A. Tschersich, Phys. Rev. B **67**, 174205 (2003).